Role of Ca diffusion in $BaZrO_3$ nanorods/$YBa_2Cu_3O_{7-x}$ multilayer nanocomposite films

Aafiya[1], Mary Ann Sebastian[2,3], Victor Ogunjimi[1], Benson Tsai[4], Abhijeet Chowdhury[4], Jialong Huang[4], Timothy Haugan[2], Haiyan Wang[4], Judy Wu[*1]

[1]*Department of Physics and Astronomy, the University of Kansas, Lawrence, Kansas 66045, USA*
[2]*U.S Air Force Research Laboratory, Aerospace Systems Directorate, WPAFB, OH 45433, USA*
[3]*University of Dayton Research Institute, Dayton, OH 45469, USA*
[4]*School of Materials Engineering, Purdue University, West Lafayette, IN 47907, USA*
*Corresponding author e-mails: jwu@ku.edu

Abstract: In a recent study to probe the effect of the pinning efficiency of $BaZrO_3$ (BZO) nanorods in BZO-doped $YBa_2Cu_3O_{7-x}$ (BZO/YBCO) nanocomposite films, Ca diffusion from two $Ca_{0.3}Y_{0.7}Ba_2Cu_3O_{7-x}$ spacers that form multilayers through alternative stacking with three BZO/YBCO layers was found to significantly enhance the pinning by approximately five folds at high magnetic fields (B) up to 9.0 T. This raises a question on the role of Ca diffused into the multilayer BZO/YBCO nanocomposite films. In order to answer this question, this work investigates the $Ca_{0.3}Y_{0.7}Ba_2Cu_3O_{7-x}$ films of variable thickness in the range of 33-190 nm to understand whether the carrier over-doping induced by Ca substitution of Y would lead to enhanced pinning. In addition, the effect of the thicknesses of the constituent YBCO and $Ca_{0.3}Y_{0.7}Ba_2Cu_3O_{7-x}$ layers was also studied. Furthermore, the amount of Ca in $Ca_{0.3}Y_{0.7}Ba_2Cu_3O_{7-x}$ spacers may be controlled by varying their thickness ranging from 1 nm to 10 nm. Our result suggests that the benefit of over-doping via Ca/Y substitution is minimal on pinning. In addition, the amount of Ca in the $Ca_{0.3}Y_{0.7}Ba_2Cu_3O_{7-x}$ spacers indeed affects the Ca diffusion and hence pinning enhancement dramatically, which reduces as the spacer thickness is below 5 nm threshold. Above this threshold, the Ca diffusion is highly effective through large BZO/YBCO thicknesses up to 330 nm (total film thickness ~ 1 μm) and significantly enhanced pinning has been obtained in multilayer BZO/YBCO nanocomposites. For example, the I_c exceeds 650 A per cm-width at 20 K and 9.0 T when B//c, which is only ~13% lower than that at B//ab due to the intrinsic pinning.

Keywords: BZO/YBCO nanocomposite film, vortex pinning efficiency, multilayer, Ca diffusion, over-doping

1. Introduction:

High critical current density (J_c) in applied magnetic fields (B) of a few to 10s of Tesla or high $J_c(B)$ is required for many practical applications of superconductors such as $YBa_2Cu_3O_{7-x}$ (YBCO). Considering the small superconducting coherence length on the order of a few nanometers, generation of impurity artificial pinning centers of comparable dimension in YBCO has been the research focus of many groups. Considering YBCO films are c-axis orientated epitaxial in the plane of the substrates, whether single-crystals such as $SrTiO_3$ or metals with epitaxial buffer layers, the impurity APCs form through phase segregation and diffusion driven by the strain field due to the lattice mismatch at the APC/YBCO interface. In an elastic strain energy model developed to explain such a self-assembly process, minimization of the strain energy in the APC/YBCO nanocomposite films leads to determination of the morphology, orientation, and dimension of APCs [1-3]. For example, at a relatively low to moderate impurity doping, one-dimensional APCs or nanorods were found to form arrays aligned along the c-axis of the epitaxial YBCO films and coated conductors while higher doping changes the orientation to ab-aligned as a consequence of the strain energy minimization. Considering the layered structure of YBCO with the weak pinning at B//c, the c-axis aligned nanorods can provide strong collective pinning at B//c-axis, which motivated exploration of impurities, such as $BaZrO_3$ (BZO) that has a large lattice mismatch of 7.7% with YBCO, to form nanorods (BZO-NRs) in YBCO [4-8].

It should be noted that the large lattice mismatch at the BZO-NRs/YBCO interface can lead to a high defective interface [9-11]. The commonly identified defects are dislocations on which oxygen deficiency is present. This means that the defective YBCO column of up to 5-10 nm in thickness around the BZO-NRs has reduced superconductivity. With increasing BZO doping, the defective YBCO columns around individual BZO nanorods will overlap, which is shown in decreasing superconducting transition temperature (T_c) with increasing BZO doping [12]. The reduced sharpness of the pinning energy across the defective BZO-NRs/YBCO interface projects a reduced specific pinning force density (F_p) of nanorods theoretically [13], which was confirmed experimentally in the measured lower F_p by nanorods of BZO than that of BHO nanorods with much reduced interface defects [10, 14, 15]. This result suggested that improving the BZO-NRs/YBCO interface may lead to enhanced F_p, which motivated us to develop a multilayer (ML) approach to dynamically enlarge the c-axis constant of YBCO column around the BZO-NRs by diffusing Ca ions from Ca-containing thin spacers grown with BZO/YBCO layers in the ML structure [16, 17]. It should be noted that Ca/Y, Ca/Ba and Ca/Cu substitutions are all possible, depending on the strain field of YBCO lattice as studied in a theoretical simulation on the Ca-doping effect of YBCO bulks [18]. Since the YBCO column around the BZO-NRs is under tensile strain, the replacement of smaller Cu+2 ions on the Cu-O planes of YBCO lattice with larger Ca+2 ions (by 30%) is hence energetically favorable as confirmed experimentally in observation of stacking faults associated to the Ca/Cu substitution on the Cu-O planes [17]. Further studies of the Ca diffusion mechanism and the impact on the pinning by changing the thicknesses of the spacers and BZO/YBCO layers will be the focus of this work.

2. Experimental

Pulsed laser deposition (PLD) was used to prepare samples of $Ca_{0.3}Y_{0.7}Ba_2Cu_3O_{7-x}$ (CaY-123) films and BZO/YBCO films on (100) $SrTiO_3$ (STO) single crystal substrates [4, 19, 20]. The PLD targets have nominal compositions of CaY-123 for the former, and 2 or 6 vol.% BZO doping in YBCO for the latter. Two CaY-123 films of 33 and 190 nm thicknesses were fabricated in this work. A set of BZO/YBCO ML samples were fabricated by growth of three BZO/YBCO layers of 50 nm in thickness alternatively with two 10 nm thick CaY-123 spacers. In this set, one sample has 2 vol.% BZO doping while the other has 6 vol.% BZO doping. In addition, a set of 6 vol.% BZO/YBCO samples were fabricated with CaY-123 spacer thickness of 1 nm, 5 nm, and 10 nm while the thickness of the three BZO/YBCO layers was fixed at 50 nm. For convenience, they are regarded as BZO/YBCO ML-1nm, BZO/YBCO ML-5nm, and BZO/YBCO ML-10nm, respectively. A summary of the information of the samples studied in this work is provided in Table 1. The PLD repetition rate of 2 Hz was adopted for CaY-123 and it was 8 Hz for BZO/YBCO. For comparison, single-layered (SL) BZO/YBCO films were also made at the same condition. Tencor P-16 profilometer was used to confirm film thicknesses of 150-160 nm on the ML and SL BZO/YBCO films in this study. During PLD, the substrate temperature was fixed at ~825 °C in

Table 1. Structural parameters of CaY-123 and BZO/YBCO SL and ML films investigated in this study.

Sample ID	CaY-123 Spacer Thickness (nm)	BZO Doping/ BZO/YBCO Layer Thickness (vol.%/nm)	BZO/YBCO Layer number	Total Film Thickness (nm)
CaY- 123	–	–	–	33
CaY- 123	–	–	–	190
2% BZO/YBCO SL	NA	2/150	1	150
2% BZO/YBCO ML	10	2/50	3	150
6% BZO/YBCO SL	NA	6/150	1	150
6% BZO/YBCO ML-1 nm	1	6/50	3	150
6% BZO/YBCO ML-5 nm	5	6/50	3	150
6% BZO/YBCO ML-10 nm	10	6/50	3	150
6% BZO/YBCO ML	10	6/150	3	450
6% BZO/YBCO ML	10	6/250	3	750
6% BZO/YBCO ML	10	6/330	3	1000

300 mTorr O_2 [4]. After the PLD deposition was completed, the oxygen pressure was increased to 760 Torr during sample cooling and annealing at ~500 °C for 0.5 hour. Scanning transmission electron microscopy (STEM, Thermo Fisher Scientific Themis-Z TEM system) was adopted to study the morphology and interface microstructure of the BZO/YBCO films. Elemental distribution across the cross-sectional area was characterized to confirm the ML structure using energy dispersive X-Ray spectroscopy (EDS). For electric transport measurement, 100 nm thick silver contacts were deposited on the films using DC magnetron sputtering. On each 5x5 mm^2 film, two microbridges were patterned using photolithography [21, 22]. The bridges are 500 μm in length and 20 or 40 μm in width. Resistance–temperature (*R-T*) and current-voltage (*I-V*) characteristic curves were taken in a Quantum Design Ever-Cool II Physical Property Measurement System (PPMS), which has temperature range of 4.2 K-400 K and *B* field up to 9.0 T. A Keithley 2430 Pulse Source Meter was utilized to generate current pulses of width of 500 ms to minimize Joule heating. 1 μV/cm standard criterion was used to determine J_c [22-24].

3. Results and Discussions

Figure 1 exhibits the accommodation field $B^* \sim n^* \Phi_0$ estimated from the areal concentration (n*) of the BZO-NRs aligned along the c-axis of the YBCO films assuming a simple square lattice of the BZO-NRs with one quantized magnetic vortex Φ_0 pinned on each BZO-NR [4, 10, 19]. With increasing BZO doping in 150 nm thick BZO/YBCO-SL films, the B^* (open) increases linearly with the increasing n*, which means the doped BZO indeed form BZO-NRs proportional to the BZO doping amount. If each BZO-NRs pins a vortex, the peak position (B_{pmax}) of the pinning force density F_p should be comparable to B^* since at $B < B^*$, all vortices would be pinned by BZO-NRs while at $B > B^*$, some of the vortices would find no strong pins to be pinned. In Figure 1, the B_{pmax} values extracted from $\boldsymbol{F_p(B) = J_c(B) \times B}$ curves measured in transport measurement on BZO/YBCO nanocomposite films are included for comparison with the B* extracted from the TEM in our previous works [4, 10, 19, 25]. The much lower B_{pmax} value at a given BZO doping than the corresponding B^* value is indicative of a substantial portion of the formed BZO-NRs not contributing to pinning. This raises a question about what prevents the formed BZO-NRs from pinning vortices efficiently.

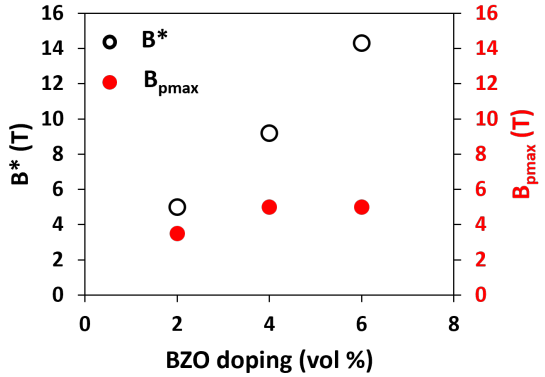

Figure 1. Comparison of the TEM-derived matching field B^* (open circles) and the transport-measured B_{pmax} (closed circles) where peak pinning force density F_p is located at 65 K (B//c) as a function of BZO doping in ~150 nm thick BZO/YBCO SL films.

In order to answer this question, we have explored fabrication of BZO/YBCO ML by inserting two Ca-containing spacer layers into a BZO/YBCO SL film. The ML films therefore have five layers grown alternatively at the sequence of BZO/YBCO (1st layer), CaY-123 (2nd layer), BZO/YBCO (3rd layer), CaY-123 (4th layer), and BZO/YBCO (5th layer). Figures 2a-b show schematically the cross-section of two BZO/YBCO ML samples (only 3 layers shown) with different spacer thicknesses of 1.0 nm and 5 nm respectively. While Ca diffusion is possible both along the BZO/YBCO interface and directly into YBCO as shown by the arrows, the former was found to provide a more efficient diffusion channel due to the interfacial strain associated to the lattice mismatch between BZO and YBCO [16,

26]. Figures 2c-d show the STEM cross-sectional view and EDS map of Ca on a BZO/YBCO ML samples, BZO-NRs are shown as black lines along c-axis of YBCO or the normal direction of the film. The defective YBCO columns around the BZO-NRs are shown in white instead of grey for YBCO with optimal oxygen. In the BZO doping of 2-6%, the diameter of the BZO-NRs remains comparable ~ 5-6 nm while the inter-rod spacing decreases monotonically. At 2 vol.% the spacing is ~ 20 nm and at 6 vol.% it decreases to ~ 12 nm [4, 10, 27]. This means the defective YBCO columns around the BZO-NRs would overlap at high BZO doping, resulting in monotonically decreasing T_c since the columns are oxygen deficient. This argument is consistent with experimentally measured T_c values in BZO/YBCO SL films. For example, T_c ~89.2 K in the 2 vol.% BZO/YBCO SL while it decreases to 86.5 K as the BZO doping increases to 8 vol.% [28].

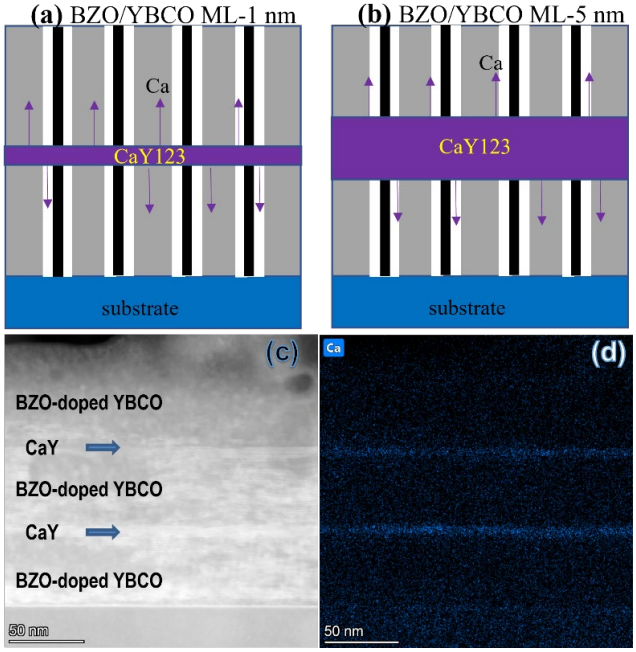

Figure 2. Schematic illustrations of (a) BZO/YBCO ML-1nm, (b) BZO/YBCO ML-5nm nanocomposite films (only three layers are shown). (c) Cross-sectional STEM image and (d) EDS map of Ca in a BZO/YBCO ML-5nm sample. The BZO/YBCO layer in (c)-(d) is about 50 nm thick.

In the ML samples, the CaY-123 spacers are used to control the amount of Ca ions that may diffuse into BZO/YBCO layers (purple arrows). This means the thickness of the spacer may determine the total amount of Ca available for diffusion. In our prior works [16, 17], we have found that the Ca ion diffusion is mostly along the BZO-NRs/YBCO interface, which is not surprising since the strain field initiates from the interface due to the lattice mismatch between BZO and YBCO. In another word, the strained interface may serve as a more effective diffusion channel for Ca ions than away from the interface. The Ca ion diffusion along the interface is followed by the Ca/Cu substitution on the YBCO lattice near the interface. Since Ca has a larger ionic radius than that of Cu ions by ~ 30%, this substitution leads to ~ 24% elongation of the YBCO lattice along the c-axis (1.17 nm), resulting in a significantly reduced BZO/YBCO lattice mismatch to ~ 1.4% and hence interface defects concentration. It should be noted that reducing the negative effect of the strain field in the ML samples is not at the cost of disturbing self-assembly of BZO-NRs since they form in an identical way in the ML (the 1st layer) and SL samples. Since the CaY-123 spacers are very thin, the modulated strain field extends through the spacers to allow the BZO-NRs in the higher BZO/YBCO layers to align with those in the 1st layer in ML samples. This means the BZO-NRs have the same diameter and concentration in the BZO/YBCO ML and SL films as confirmed experimentally [16, 17]. However, the ML approach allows a coherent BZO-NRs/YBCO interface to be obtained as confirmed in STEM studies [16, 17]. Since the spacers would truncate BZO-NRs into short segments, smaller spacer thickness is hence preferred to allow BZO-NRs to be well aligned through the film thickness with the highest pinning efficiency. On

the other hand, the amount of Ca available for diffusion is proportional to the spacer thickness. An optimal spacer thickness would encourage the growth of aligned BZO-NRs with adequate Ca diffusion into the entire BZO-NRs/YBCO interface.

The BZO/YBCO ML films showed a similar but slightly more decreasing T_c with increasing BZO doping to their SL counterparts. This means an additional mechanism, possibly over-doping of YBCO via Ca/Y substation. For example, the T_c of 84.0 K for the 6 vol.% BZO/YBCO ML film is 2.9 K lower than its SL counterpart's. The slightly reduced T_c values in the ML samples are outweighed by the much-enhanced J_c (B) and F_p (B) due to the Ca-induced BZO-NRs/YBCO interface repair and the consequent pinning efficiency recovery. The F_p (B) curves measured on 2 vol.% (Figure 3a) and 6 vol.% (Figure 3b) BZO/YBCO SL and BZO/YBCO ML samples, respectively, are compared at 65 K at B//c. In the entire B field range up to 9.0 T, it is apparent that the ML samples (filled) outperform their SL counterparts (open). It should be mentioned that reduced pinning force per BZO-NR length was reported in multilayer YBCO structures, which can be attributed to reduced BZO-NR length by the non-Ca-containing YBCO spacers [29-31]. Using the CaY-123 spacers, an opposite trend of higher J_c (B) and F_p (B) achieved in the ML films may be attributed to dynamic elongation of the c-axis of YBCO columns around the BZO-NRs during the film growth to effectively suppress the formation of oxygen-deficient defects in these columns associated to the original strain field initiated from the large lattice mismatch at the BZO-NRs/YBCO lattice [32-35]. By diffusing Ca ions from the CaY-123 spacers along the BZO-NRs/YBCO interface followed with Ca/Cu substitution allows reduction or elimination of these defects in the ML samples. Quantitatively, the peak values of F_P (B) curves or $F_{p,max}$ are indicated by the arrows inside Figure 3. At 2 vo.% BZO doping, the $F_{p,max}$ of 98 GNm^{-3} for the ML sample is about 170% of 57 GNm^{-3} for the SL counterpart [8, 36-38]. A more significant enhancement was observed in the 6 vol.% BZO doping case. Specifically, the $F_{p,max}$ of ~160 GN/cm^3 in the ML sample is about 500% of its SL counterpart's. Besides the enhanced F_p (B), the B_{max} values in ML samples are comparable to that of the SL counterparts' at lower BZO doping while considerably higher at higher BZO doping. This means that the Ca ion diffusion and Ca/Cu substitution on YBCO lattice lead to not only enhanced pinning efficiency of individual BZO-NRs but also the portion of the formed BZO-NRs contributing to pinning.

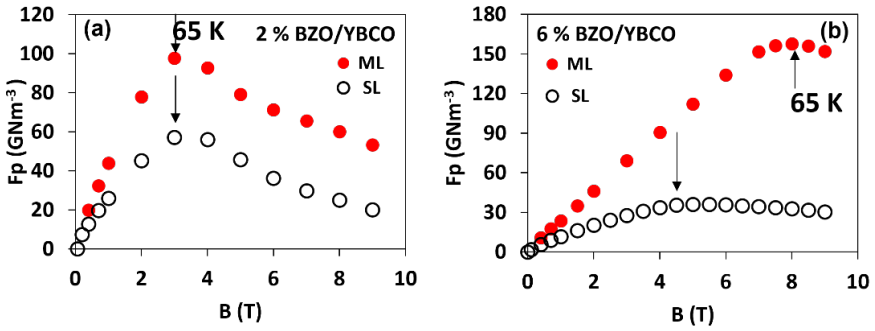

Figure 3. F_p as a function of B field for (a) 2 vol.% and (b) 6 vol.% BZO/YBCO SL (open circles) and ML-10nm (filled circles) nanocomposite samples. The arrows mark the B_{pmax} locations. The SL sample has a single BZO/YBCO layer of 150 nm thickness, while the ML sample has a total BZO/YBCO thickness of 150 nm consisting of three layers of 50 nm each.

Figure 4a exhibits the resistance-temperature (R-T) and F_p(B) curves at 50 K on the 190 nm thick CaY-123 films. The low T_c~72 K is anticipated due to over-doping by substitution of Y with Ca on YBCO, which also prohibited J_c (B) and F_p (B) to be measured at high temperatures such as 65 K. At 50 K, the low F_p (B) on this sample and another sample of smaller thickness of 33 nm with even lower T_c~67 K rule out the contribution of the spacers directly to the enhanced pinning in the ML samples. This is not surprising. While improved pinning in self-field may be associated to the over-doping, the lack of pinning centers in the CaY-123 spacers explains the low F_p (B). This confirms that the major role of the CaY-123 spacers is to provide Ca ions to allow them to diffuse into the tensile-strained BZO-NRs/YBCO interface, followed by dynamically enlarging the c-axis of YBCO column around the BZO-NR and reducing the interface lattice mismatch and hence interface defects for enhanced pinning efficiency of BZO-NRs.

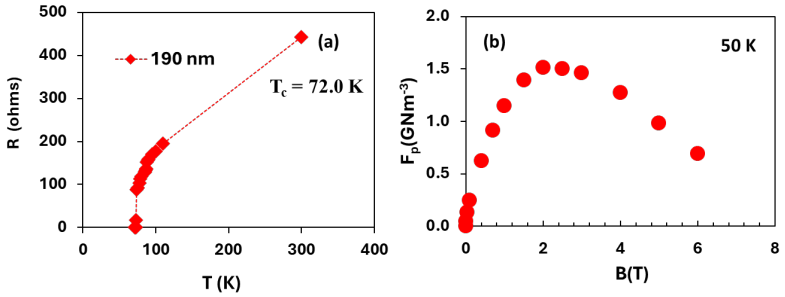

Figure 4. (a) R-T curve exhibiting T_c~72 K, and (b) F_p-B curve measured on a 190 nm thick CaY-123 spacer layer sample at 50 K.

Figure 5a compares the F_p (B) curves on three 6 vol.% BZO/YBCO ML samples with CaY-123 spacers of different spacer thickness of 1 nm (diamonds), 5 nm (triangles) and 10 nm (circles). The trend of lower enhancement of F_p (B) at smaller spacer thickness confirms that Ca ion diffusion is indeed associated with the amount of Ca in spacers. Among the three, 10 nm thick spacer has the highest F_p (B) enhancement while reducing the thickness to 5 nm or lower leads to moderate differences in F_p (B). Figure 5b compares the F_p (B) curves taken at 65 K on 6 vol.% BZO/YBCO ML films of total thicknesses of 150 nm (circles), 450 nm (triangles), 750 nm (squares), and 1000 nm (diamonds) while keeping a fixed 10 nm thickness for the two CaY-123 spacers. The slightly lower F_p (B) on thicker BZO/YBCO ML films seems to suggest less than optimal Ca ion amount as the BZO/YBCO layers are thicker. However, this trend is reversed at lower temperatures. At 50 K, the three thicker ML films have comparable J_c (B) and F_p (B) that are considerably higher than the thinner ML as temperatures are lowered further [39, 40]. The high F_p means that high critical current I_c can be obtained in thicker ML samples as observed experimentally. For example, the I_c/cm-width of the 1000 nm thick ML film is up to 465 (B//c) and 660 (B//ab) A/cm-width at 30 K and 9.0 T and as the temperature is decreased to 20 K, they increased to 654 (B//c) and 753 (B//ab) respectively.

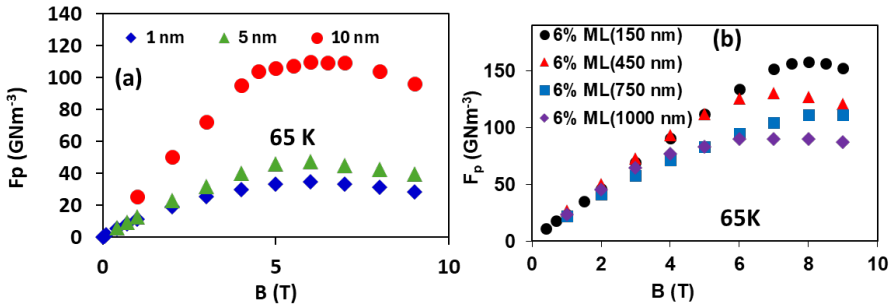

Figure 5. (a) F_p as function of magnetic field B measured at 65 K on 6 vol% BZO/YBCO ML-10nm (circles), 6 vol% BZO/YBCO ML-5nm (triangles) and 6 vol% BZO/YBCO ML-1nm (diamonds) nanocomposite samples. All samples have the five-layer structure with two CaY-123 spacers stacked with three 50 nm thick BZO/YBCO layers alternatively. (b) F_p (B) measured on 6 vol.% BZO/YBCO ML films with total thicknesses of 150 nm (circles), 450 nm (triangles), 750 nm (squares), and 1000 nm (diamonds). In all cases, the two CaY-123 spacers are 10 nm thick. The three BZO/YBCO layers have thicknesses of 50 nm each for the 150 nm film, 150 nm each for the 450 nm film, 250 nm each for the 750 nm film, and 330 nm each for the 1000 nm film.

4. Conclusions

In summary, this work presents a study to probe the diffusion mechanism of Ca ions from CaY-123 spacers to BZO/YBCO layers and their role in improving vortex pinning in 2 and 6 vol.% BZO/YBCO ML nanocomposite films. A few interesting insights have been obtained. First, the thickness of the CaY-123 spacers controls the amount of Ca ions available for diffusion. In a comparison of F_p (B) curves measured in 6 vol.% BZO/YBCO ML films with two CaY-123 spacers of thickness in the range

of 1.0 nm-10 nm, the pinning enhancement is more at higher spacer thickness. CaY-123 films of 33 nm and 190 nm thick were investigated, which showed the expected low T_c values of 67 K and 72 K respectively due to over-doping. The lower F_p (B) of the CaY-123 films than that in the BZO/YBCO SL and ML films by orders of magnitude rules out the contribution of the CaY-123 spacers to pinning as a possible mechanism underlying the enhanced pinning in BZO/YBCO ML films. When applying the same five-layer structure for thicker ML samples with the thickness in the range of 150-1000 nm, comparable enhanced pinning at 65 K and more enhanced pinning at lower temperatures on thicker ML samples was obtained using the same two 10 nm thick CaY-123 spacers. This result suggests the longer deposition time used for thicker ML film fabrication can facilitate Ca ion diffusion through thicker BZO/YBCO layers while further improvement may be possible by optimizing the ML structure and PLD condition.

Acknowledgement
This research was supported in part by NSF contracts Nos: NSF-DMR-2413044, the AFRL Aerospace Systems Directorate, the Air Force Office of Scientific Research (AFOSR LRIR # 24RQCOR004). J. S. and H.W. acknowledge the support from the U.S. Office of Naval Research (ONR, No. N00014-20-1-2600) and the U.S. National Science Foundation (No. DMR-2016453) for the TEM/STEM work.

References

1. Wu, J. and J. Shi, *Interactive modeling-synthesis-characterization approach towards controllable in situ self-assembly of artificial pinning centers in RE-123 films.* Supercon. Sci. and Tech., 2017. **30**(10): p. 103002.
2. Shi, J.J. and J.Z. Wu, *Micromechanical model for self-organized secondary phase oxide nanorod arrays in epitaxial YBa2Cu3O7− δ films.* Philosophical Magazine, 2012. **92**: p. 2911.
3. Shi, J.J. and J.Z. Wu, *Influence of the lattice strain decay on the diameter of self assembled secondary phase nanorod array in epitaxial films.* J. of Applied Physics, 2015. **118**, p.164301
4. Baca, F.J., et al., *Interactive Growth Effects of Rare-Earth Nanoparticles on Nanorod Formation in YBa2Cu3Ox Thin Films.* Advanced Functional Materials, 2013. **23**(38): p. 4826.
5. Chen, S., et al., *Enhancement of isotropic pinning force in YBCO films with BaZrO3 nanorods and Y_2O_3 nanoparticles.* IEEE Trans. Appl. Supercond, 2017. **27**(4): p. 4-8.
6. MacManus-Driscoll, J., et al., *Strongly enhanced current densities in superconducting coated conductors of YBa 2 Cu 3 O 7–x+ BaZrO 3.* Nature materials, 2004. **3**, 439.
7. Matsumoto, K. and P. Mele, *Artificial pinning center technology to enhance vortex pinning in YBCO coated conductors.* Superconductor Science and Technology, 2009. **23**(1): p. 014001.
8. Wee, S.H., et al., *Engineering nanocolumnar defect configurations for optimized vortex pinning in high temperature superconducting nanocomposite wires.* Sci. Rep, 2013. **3**: p. 2310.
9. Foltyn, S., et al., *Materials science challenges for high-temperature superconducting wire.* Nature Materials, 2007. **6**(9): p. 631.
10. Gautam, B., et al., *Probing the effect of interface on vortex pinning efficiency of one-dimensional BaZrO3 and BaHfO3 artificial pinning centers in YBa2Cu3O7-x thin films.* Applied Physics Letters, 2018. **113**(21): p. 212602.
11. Wu, J., et al., *Pinning Efficiency of One-Dimensional Artificial Pinning Centers in YBa 2 Cu 3 O 7-x Thin Films*. IEEE Transactions on Applied Superconductivity, 2019. **29**(5): p. 1-5.
12. Cantoni, C., et al., *Strain-driven oxygen deficiency in self-assembled, nanostructured, composite oxide films.* ACS nano, 2011. **5**(6): p. 4783-4789.
13. Blatter, G., et al., *Vortices in high-temperature superconductors.* Reviews of Modern Physics, 1994. **66**: p. 1125.
14. Ogunjimi, V., et al. *The effect of APC/YBCO interface on the angular range of effective pinning by one-dimensional artificial pinning centers in $YBa_2Cu_3O_{7-x}$ nanocomposite films*. IOP Conference Series: Materials Science and Engineering, 2020. **756**(1): p. 012025.
15. Ogunjimi, V., et al., *The angular range of effective pinning by one-dimensional artificial pinning centers in $BaZrO_3$/ $YBa_2Cu_3O_{7-x}$ nanocomposite films.* AIP Adv., 2019. **9**: p. 085110.
16. Wu, J.Z., et al., *Enabling coherent $BaZrO_3$ nanorods/$YBa_2Cu_3O_{7-x}$ interface through dynamic lattice enlargement in vertical epitaxy of $BaZrO_3$/$YBa_2Cu_3O_{7-x}$ nanocomposites.* Supercon. Sci. and Tech., 2022. **35**(3): p. 034001.

17. Ogunjimi, V., et al., *Enhancing Magnetic Pinning by $BaZrO_3$ Nanorods Forming Coherent Interface by Strain-Directed Ca-doping in $YBa_2Cu_3O_{7-x}$ Nanocomposite Films.* Supercon. Sci. and Tech., 2021. **34**(10): p. 104002.
18. Klie, R.F., et al., *Enhanced current transport at grain boundaries in high-T-c superconductors.* Nature, 2005. **435**(7041): p. 475-478.
19. Baca, F.J., et al., *Control of $BaZrO_3$ nanorod alignment in $YBa_2Cu_3O_{7-x}$ thin films by microstructural modulation.* Applied Physics Letters, 2009. **94**(10): p. 102512.
20. Sebastian, M.A., et al., *Comparison Study of the Flux Pinning Enhancement of $YBa_2Cu_3O_{7-x}$ Thin Films With $BaHfO_3$ + Y_2O_3 Single- and Mixed-Phase Additions.* IEEE Trans. Appl. Supercond., 2019. **29**(5): p. 1-5.
21. Wang, X., et al., *Eliminating thickness dependence of critical current density in $YBa_2Cu_3O_{7-x}$ films with aligned $BaZrO_3$ nanorods.* J. of Applied Physics, 2010. **108**(11): p. 3911.
22. Chen, S., et al., *Enhancement of Isotropic Pinning Force in YBCO Films With $BaZrO_3$ Nanorods and Y_2O_3 Nanoparticles.* IEEE Trans. Appl. Supercond., 2017. **27**, p. 1-5.
23. Gautam, B., et al., *Microscopic Adaptation of $BaHfO_3$ and Y_2O_3 Artificial Pinning Centers for Strong and Isotropic Pinning Landscape in $YBa_2Cu_3O_{7-x}$ Thin Films.* Supercon. Sci. and Tech., 2018. **31**(2): p. 025008.
24. Emergo, R.L.S., et al., *The effect of thickness and substrate tilt on the BZO splay and superconducting properties of $YBa_2Cu_3O_{7-x}$ films.* Superc. Sci. and Tech., 2010. **23**, p. 115010.
25. Panth, M., et al., Multilayer $YBa_2Cu_3O_{7-x}$/$Ca_{0.3}Y_{0.7}Ba_2Cu_3O_{7-x}$ Nanocomposite Films With 2–8% $BaZrO_3$ Doping for High-Field Applications. IEEE Trans. Appl. Supercond., 2022. 32(8): p. 1-8.
26. Wu, J., et al., *Artificial Pinning Centers and the Quest of High Critical Current Densities in HTS Nanocomposites.* IEEE Trans. Appl. Supercond., 2023. **33**(5): p. 1-8.
27. Baca, F., et al., *Control of BaZrO3 nanorod alignment in YBa2Cu3O7-x thin films by microstructural modulation.* Applied Physics Letters, 2009. **94**(10): p. 2512.
28. Wu, J., et al., *Ca-repaired $BaZrO_3$ nanorods/$YBa_2Cu_3O_{7-x}$ interface for enhanced pinning in $YBa_2Cu_3O_{7-x}$ nanocomposites with 2-8% $BaZrO_3$ doping.* IOP Conference Series: Materials Science and Engineering, 2024. **1302**(1): p. 012013.
29. Horide, T., M. Ishimaru, and K. Matsumoto, *Observation of inhomogeneous depinning in $YBa_2Cu_3O_{7-x}$ composite multilayers.* Supercon. Sci. and Tech., 2019. **32**(8): p. 085001.
30. Horide, T., et al., *Hybrid artificial pinning centers of elongated-nanorods and segmented-nanorods in $YBa_2Cu_3O_{7-x}$ films.* Supercon. Sci. and Tech., 2016. **29**(10): p. 105010.
31. Malmivirta, M., et al., *Enhanced flux pinning in YBCO multilayer films with BCO nanodots and segmented BZO nanorods.* Scientific reports, 2017. **7**(1): p. 1-8.
32. Horide, T., et al., *Structural Evolution Induced by Interfacial Lattice Mismatch in Self-Organized $YBa_2Cu_3O_{7-x}$ Nanocomposite Film.* ACS nano, 2017. **11**(2): p. 1780-1788.
33. Shi, J.J. and J.Z. Wu, *Structural transition of secondary phase oxide nanorods in epitaxial $YBa_2Cu_3O_{7-x}$ films on vicinal substrates.* Philosophical Magazine, 2012. **92**(34): p. 4205.
34. Wu, J.Z., et al., *The effect of lattice strain on the diameter of BaZrO3 nanorods in epitaxial $YBa_2Cu_3O_{7-x}$ films.* Supercon. Sci. and Tech., 2014. **27**(4): p. 044010.
35. Yoshida, Y., et al., *Approaches in controllable generation of artificial pinning center in REBCO coated conductor for high-flux pinning.* Supercon. Sci. and Tech., 2017. **30**, 104002.
36. Huhtinen, H., et al., *The effect of BZO doping concentration and thickness dependent properties of YBCO films grown by PLD on buffered NiW substrates.* Physica C: Superconductivity, 2012. **472**(1): p. 66-74.
37. Huhtinen, H., et al., *Influence of $BaZrO_3$ dopant concentration on properties of $YBa_2Cu_3O_{7-x}$ films in magnetic fields up to 30 T.* Journal of Applied Physics, 2010. **107**(5): p. 053906.
38. Jha, A.K., et al., *Tailoring the vortex pinning strength of YBCO thin films by systematic incorporation of hybrid artificial pinning centers.* Supercon. Sci. and Tech., 2015. **28**, 114004.
39. Ogunjimi, V., et al., *Attainment of high critical current in thick BaZrO3-doped $YBa_2Cu_3O_{7-x}$ multilayer nanocomposite films.* Journal of Applied Physics, 2024. **136**(15): p. 155302.
40. Wu, J., et al., *Achieving High Jc in High Fields in Multilayer BZO/YBCO Thick Films.* IEEE Transactions on Applied Superconductivity, 2025. **35**(5): p. 1-6